Chapter 5

Simulations and results

The numerical method described in Chapter 3 solves the evolution of the flow field and the coupled dynamic behavior of a sphere moving in the flow. When there is an additional solid boundary (a solid wall) existing in the flow field, the impact and rebound behavior of the sphere can be calculated by including the contact model introduced in Chapter 4. The experiments presented in Chapter 2 provide an effective validation for the proposed contact model since the sphere is released from zero velocity under quiescent ambient fluid condition, which makes the initial condition for the simulation easy to enforce. Thus the numerical simulations for the different experimental cases are performed with the corresponding initial conditions and material properties described in Chapter 2. After comparing the calculated trajectory with different δ_{ss} to the measured result in a single case, a unique value for δ_{ss} that results in the best fit to the experimental trajectory is chosen to complete the proposed contact model. The accuracy of the contact model over different Reynolds numbers is discussed by comparing trajectories and calculating the difference on the maximum height achieved in rebound process. Besides the particle trajectories, the velocity profiles, the evolution of the vorticity distribution of the flow field and the coefficient of restitutions are also investigated.

5.1 Simulation setup

To simulate the settling process of a sphere and the evolution of the surrounding flow field as described in the experiments in Chapter 2, a three-level computational multi-domain is used to enforce the same boundary conditions as used in the experiments as shown in figure (5.1). The

releasing surface and the target wall are represented with two segments fixed in the computational domain which make two plates in the axisymmetric system. A half circle which represents the sphere is initially placed $2dz$ away from the releasing surface to avoid a direct contact of the two solid bodies that may cause a singularity problem in simulation, where $dz = dr = 0.01D$ is the uniform grid size for the first level computational domain in figure 5.1(a)) For the second level computational domain (figure 5.1(b)) that is twice the size of the first domain, the grid size is $dz_2 = dr_2 = 2dz = 0.02D$. Similarly, the grid size for the third level domain is $dz_3 = dr_3 = 2^{(3-1)}dz = 0.04D$ (figure 5.1(c)). A far field boundary condition (slip but non-penetrating) is applied at the boundary of the third level computational domain as required by the numerical method. For the symmetric axis $r = 0$, the boundary condition is strictly satisfied. For the other three boundaries, the slip-non-penetrating boundary condition for the large domain with coarser mesh is appropriate since the tank used in the experiments is large and accordant with the third domain.

The coupled systems are non-dimensionalized with characteristic length, the diameter of the sphere, $L_o = D$, and characteristic time $t_o = \sqrt{D/g}$ where $g = 9.8$ m/s^2 is the gravitational acceleration. The Navier-Stokes equations have a non-dimensional parameter $Re_g = D\sqrt{Dg}/\nu$ and the velocity variable can be non-dimensionalized by $\sqrt{Dg}$. For the different experiments described in Table (2.2), the Reynolds number, Re_g, for the Navier-Stokes equations are slightly different since although the same sphere is used in these different cases but the dynamic viscosity of the liquid changes slightly when room temperature varies. The initial distance of the sphere from the target wall is different in the experiments. Correspondingly, the position of the target wall is defined at different value in the simulation for different case. In the equation of the sphere motion, the density ratio of the sphere to the liquid, $\tau = \rho_p/\rho_l$, also varies slightly with the temperature. The simulations start from $t = 0$ when the sphere is $0.02D$ away from the releasing surface with zero velocity and the flow field is static. The effect of gravity and buoyancy results in an acceleration and the sphere starts to move. The motion is coupled with the evolution of the flow field with a second order Runge-Kutta method as discussed in Chapter 3. The analytical formulas with the wall correction terms for the hydrodynamic forces are not used when the sphere is just released from the

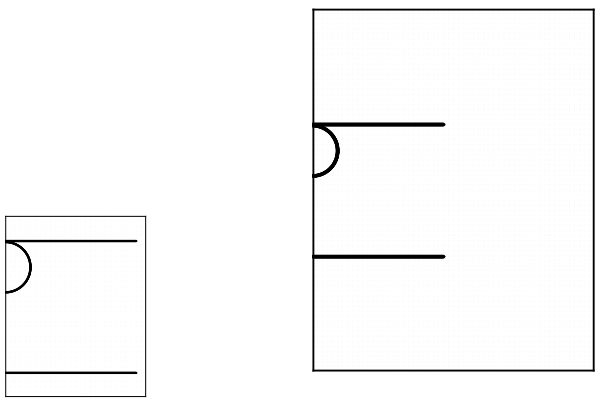

(a) grid level 1

(b) grid level 2

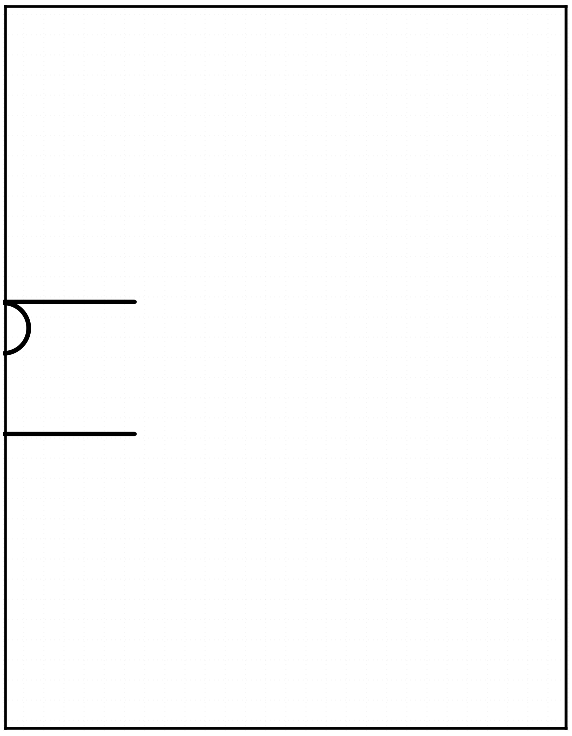

(c) grid level 3

Figure 5.1: The initial setup for the 3-level multi-domain.

releasing surface since the velocity of the sphere is very small, which makes the dominant drag force much smaller than the result when the sphere is about to collide with the target wall.

5.2 Calibration of δ_{ss}

The non-dimensional parameter δ_{ss} from the contact model plays an important role in the simulation for a collision process. As explained in Chapter 4, δ_{ss} is the threshold distance where the elastic-like force starts to take effect. When $\delta < \delta_{ss}$, the elastic-like force becomes dominant since its magnitude is very large compared with the other hydrodynamic forces and gravity. The velocity of the sphere decreases rapidly and becomes negative (sphere moves in opposite direction) under the effect of the elastic-like force. Thus, the value of δ_{ss}, influences the rebound trajectory of the sphere. The effect of δ_{ss} on the collision process is shown in figure (5.2).

In figure (5.2), the computed trajectories from simulations of the experimental case 3 with different values of δ_{ss} are compared. The vertical and horizontal axes represent the dimensionless gap between the sphere and the wall, δ and the dimensionless time, t, respectively. The value of δ_{ss} is taken to be small, ranging from $0.016D$ to $0.020D$, since the elastic force is irrelevant until the two solid surfaces are very close to each other. The first impacting process is not affected by the value of δ_{ss}. However, the rebound trajectory is different. Larger values of δ_{ss} result in smaller maximum height achieved in the rebound process.

To calibrate the value of δ_{ss}, the trajectory measured from the experiment case 3 is compared with the simulated result, as shown in figure (5.3). To distinguish the experimental points, the experimental data are presented in 2 ms time interval omitting the intermediate points. The simulation using $\delta_{ss} = 0.017$ gives the best fit for the first two rebounds. Thus $\delta_{ss} = 0.017$ is used to complete the proposed contact model. The adequacy of this value for the other collisions with different Reynolds numbers is investigated in the following section.

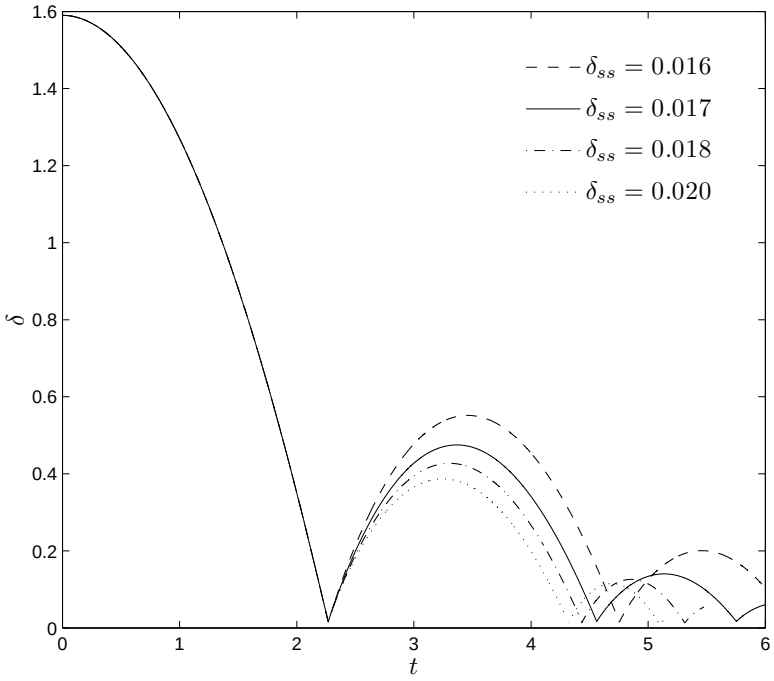

Figure 5.2: The simulated particle trajectories of case 3 with different $\delta_{\rm ss}$

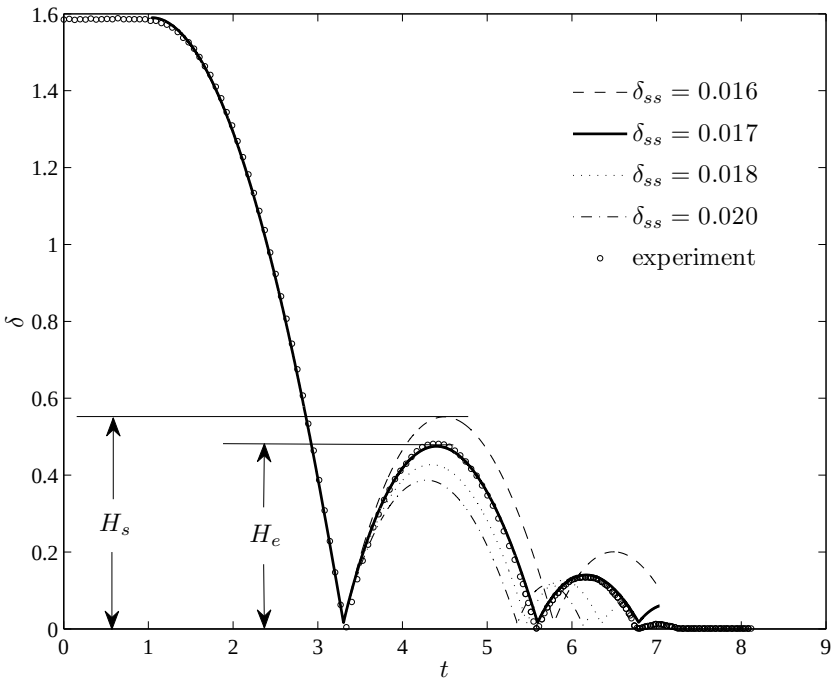

Figure 5.3: Comparison of the simulated trajectory to the measured trajectory of case 3

5.3 Particle velocity profile

The velocity profile for a sphere falling under gravity toward a solid wall in a viscous liquid environment is obtained from a numerical simulation with the contact model. The velocity decreases that have been observed in the current experiments are found in the simulated result.

Figure (5.4) shows the particle velocity in case 3 as a function of the gap between the particle and the wall. The velocity has been non-dimensionalized by $\sqrt{Dg}$. In figure 5.4(a), the particle starts to fall from $\delta = 1.6$ with zero velocity. The velocity increases as the gap decreases. The dashed line is an analytical result when only the gravitational and buoyancy forces are considered under the same initial condition. Thus, the difference between the solid line and the dashed line shows the viscous effect of the surrounding liquid on the motion of the particle. Figure 5.4(b) shows the enlarged details when the particle is about to collide with the wall. The impact velocity begins to decrease well before δ reaches δ_{SS}, where the elastic-like force resulting from the approaching of the two solid surfaces starts to take effect. This decrease in velocity results from the liquid-solid force that increases sharply as the gap, δ, diminishes. The particle decelerates before it rebounds. This phenomenon was observed in the current experiments, and also found in the experiments of Joseph *et al.* (2001) and the simulations of Ardekani & Rangel (2008). As the gap decreases to less than δ_{SS}, the elastic-like force stops the approach of the particle and makes it rebound. The rebound velocity has a sudden decrease after $\delta > \delta_{\text{SS}}$ that is shown in figure 5.4(c). The reason is because the elastic-like force falls to zero and the liquid-solid forces that always resist the sudden change of the relative velocity increases the viscous dissipation as more of the surrounding liquid re-enters the growing gap between the particle and the wall.

5.4 Qualitative flow features

The numerical simulation with the contact model captures not only the dynamics of the particles but also the evolution of the surrounding flow field during the falling and rebounding process. For the experimental case 7, figure 5.5(b) shows the snapshots of the vorticity field of the flow around

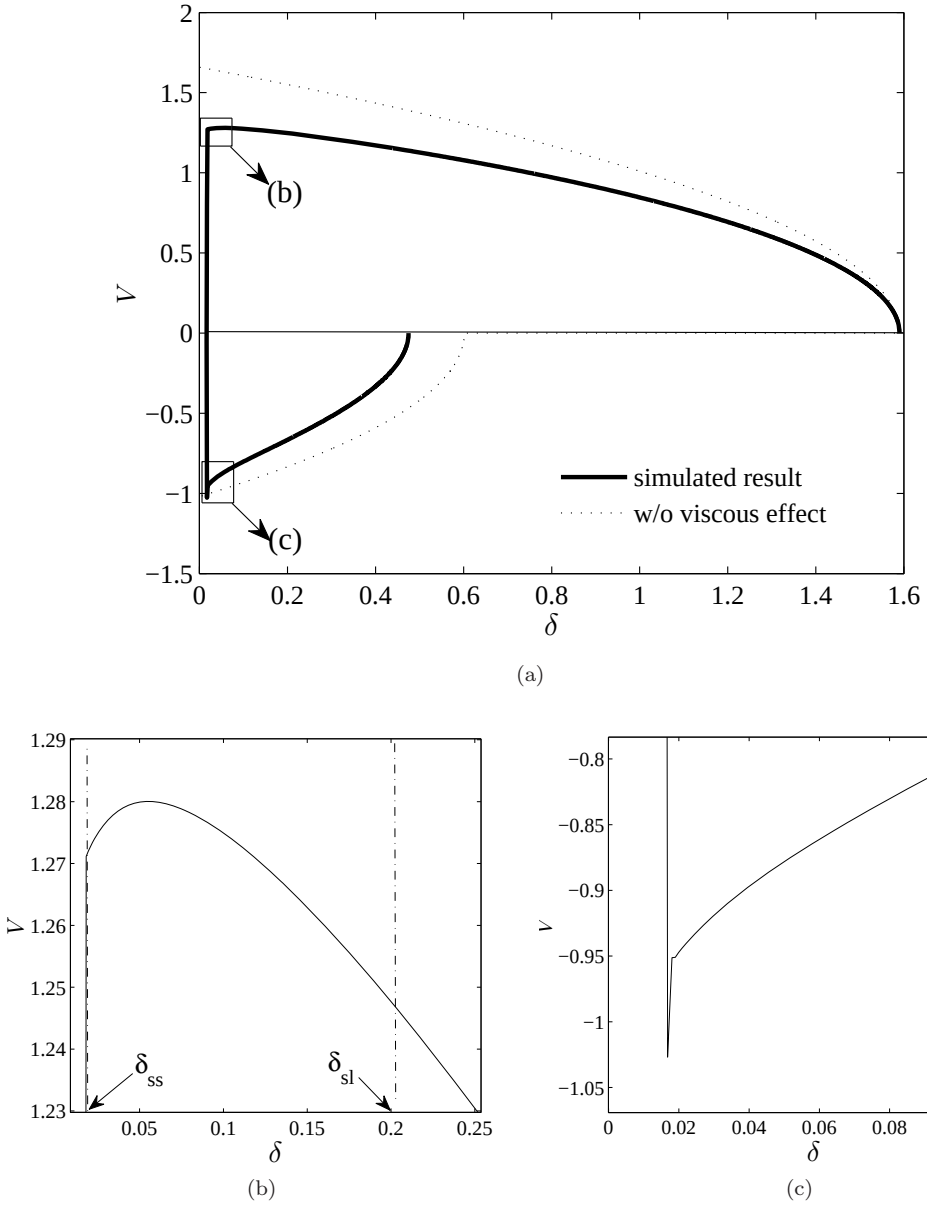

Figure 5.4: Velocity of the incoming and outgoing particle as a function of the gap between the particle and the wall. The solid line is the simulated result for case 3. The dashed line is the analytical result when just considering gravity and buoyancy effect on the particle and no liquid viscous effect. (b) and (c) present the enlarged details of the portions of (a) circumscribed in black rectangular boxes.

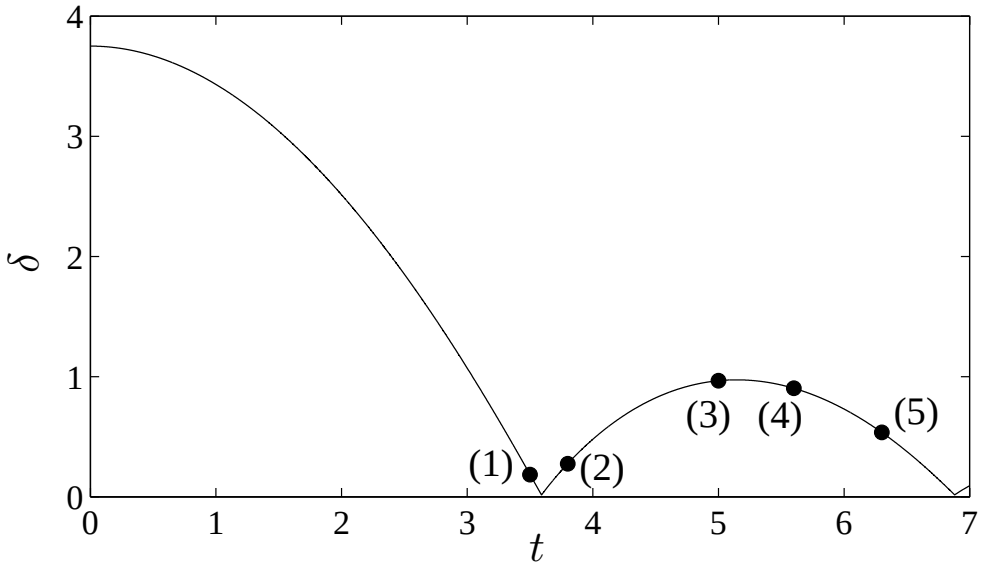

(a) particle trajectory

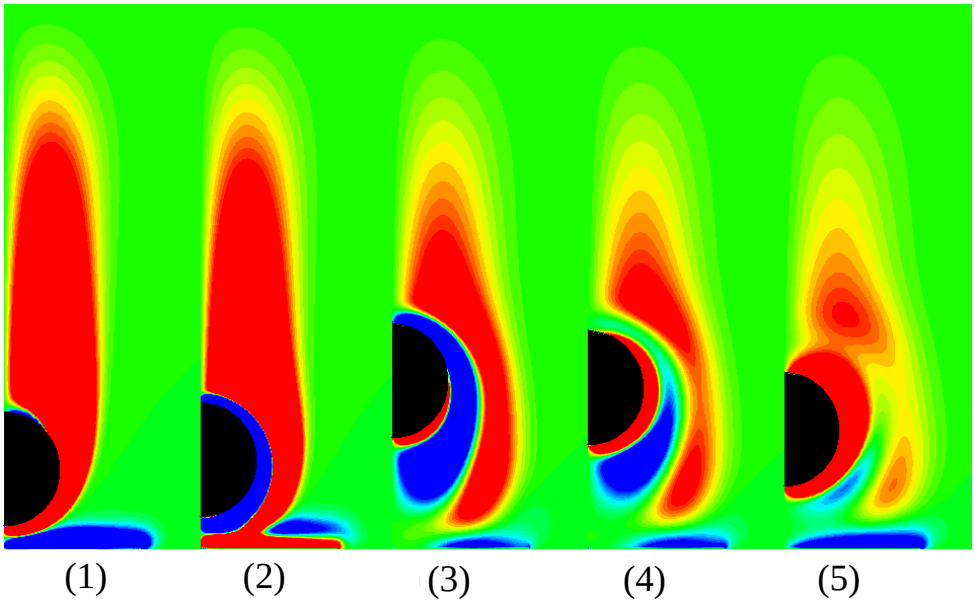

(b) Vorticity field

Figure 5.5: Snapshots of the vorticity field around the sphere at different time. Contour levels from -0.5 to 0.5 in increment of 0.05 are chosen for a good depiction of the weak vorticity field structure. The black semicircular area shows the location of the sphere. A smaller target wall is used and the release surface is omitted in this simulation.

the sphere at different times corresponding to the points on the trajectory in figure 5.5(a). The particle Reynolds number of the first impact is 134. Unlike the study of vorticity dynamics in Thompson, Leweke & Hourigan (2007) that prescribed the velocity of the sphere at a constant value and did not include the rebound, the current simulation solves the vorticity field when the sphere accelerates, decelerates and reverses directions. The first snapshot shows the primary vortex ring generated from the wake vorticity and the opposite-sign vorticity generated at the wall when the particle is just about to collide. The second snapshot is taken during the rebound after the first collision. The vorticity of opposite sign generates at the sphere surface as the rebounding sphere moves upwards through the primary wake ring to form a secondary vortex ring. Near the wall, the new vorticity forms as the result of the liquid re-entering the gap. As the sphere continues moving upwards, the primary vorticity is stretched and expanded as the sphere passes. A vortex-ring dipole forms from the combination of the primary and the secondary vorticity structures. The new positive vorticity attached to the bottom of the sphere shown in the third snapshot is formed because the sphere's velocity decreases to zero as it approaches the maximum height of the first rebound. When the sphere starts to fall again, the attached vorticity becomes a new stronger primary ring. The secondary vorticity is slowly dissipated by the surrounding opposite-sign vortices and the original primary vortex ring propagates radially before being stretched and merged with the new primary vorticity, as shown in the fourth and the fifth snapshots. The complex vorticity structure entangles the particle and dissipates a part of its kinetic energy.

5.5 Validation of the contact model

When the proposed contact model with the picked value $\delta_{\text{ss}} = 0.017$ is applied to the collision processes with different Reynolds numbers in the experimental cases 1-7, the trajectories calculated from the simulation show good agreement with the experimental results for most of the cases. To estimate the deviation, a relative error defined as $\eta = (H_s - H_e)/H_e$ is used where H_s and H_e are the maximum height that the particle reached during rebound in the simulation and in the experiment, respectively, as indicated in figure (5.3).

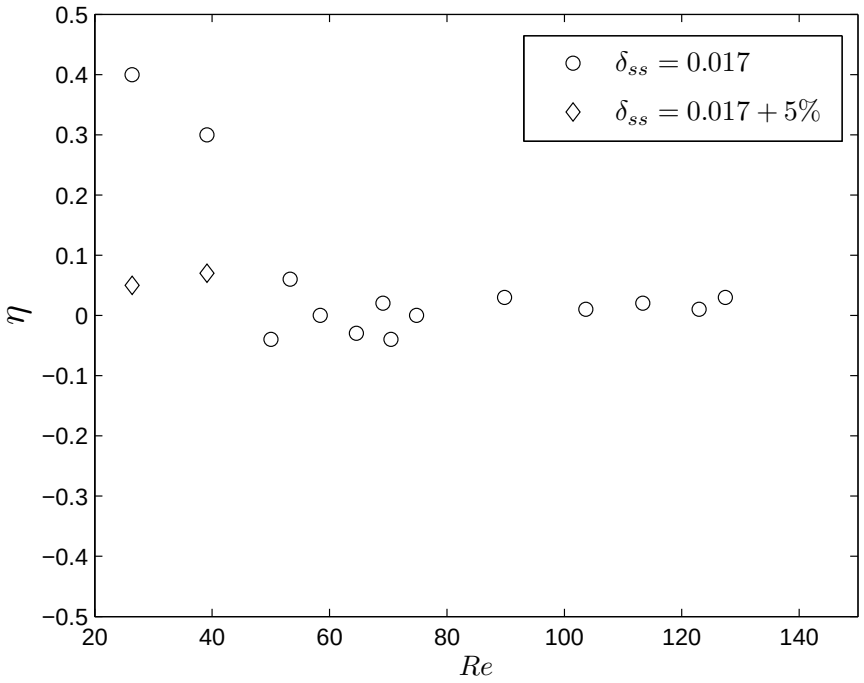

Figure 5.6: Relative error η based on maximum rebound height.

Figure (5.6) shows the relative error for the first and second impacts for each case. For the cases with Reynolds numbers ranging from 50 to 140, the relative error is small and within the uncertainty of the experiments. For smaller Re number, such as $Re = 29$, the simulation with $\delta_{\text{ss}} = 0.017$ results in a higher rebound than found in the experiment. The inaccuracy at low Re numbers is also seen in the third rebound in figure (5.3). To simulate the measured trajectory for lower Reynolds number, larger values of δ_{ss} are tried in different simulations since, as discussed in the previous section, a larger δ_{ss} results in a lower maximum height achieved in a rebound. The results are also shown in figure (5.6), which confirms that the relative error decreases when a larger δ_{ss} is used. With a 5% increase in δ_{ss}, the relative error falls within the uncertainty of the experimental region. The reason is discussed in section 5.7.

5.6 Discussion of the parameter δ_{ss}

In the current simulations, the calculated results are influenced by the value of the non-dimensional parameter δ_{ss} taken in the contact model. For Stokes number larger than 30, the simulations with $\delta_{ss} = 0.017$ produce the good agreement with experimental results for the trajectory and the coefficient of restitution. For Stokes number less than 30 but larger than 10 (runs 18-20 and runs 30-32), the simulation predicts a higher coefficient of restitution when using $\delta_{ss} = 0.017$; a lower coefficient of restitution that agrees with the experimental result is obtained when using $\delta_{ss} = 0.017 + 5\%$. The combined effect of the liquid-solid interaction and the elastic force terms is believed to be the reason. From equations (4.18) and (4.19), the elastic-like force depends on the impact velocity at δ_{ss}. In simulations with Stokes number less than 30, when $\delta_{ss} < \delta < \delta_{sL}$, the particle velocity decreases remarkably because of the effect of the liquid-solid interaction term, as discussed in section 5.3. Thus, a smaller impact velocity results in a smaller elastic force that leads to lower dissipation and a higher rebound velocity. When using $\delta_{ss} = 0.017 + 5\%$ (runs 30-32), the elastic force term is activated earlier where the particle velocity is larger than the value at $\delta_{ss} = 0.017$. As a result, W_o is larger and the larger elastic-like term results in large deceleration. The combined effect of the liquid-solid interaction term and the elastic term provides more dissipation for the collision process. The results of coefficient of restitution for runs 25-28 fall within the experimental uncertainty. This kind of influence is hidden for Stokes number greater than 30 since the particle inertia is larger and the liquid has less viscous effect.

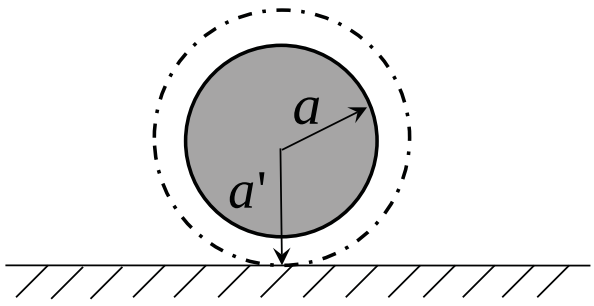

Figure 5.7: Schematic effective radius

The physical meaning of δ_{ss} can be explained by employing a concept of 'effective radius'. As

a sphere is about to collide onto a wall, the hydrodynamic pressure building up in the fluid layer between the two solid surfaces becomes large. Under the extreme pressure, the approaching solid surfaces deform elastically even before the real contact occurs (Davis *et al.* (1986)). Also, it is expected that the fluid may also compress and its density and viscosity may increases. Barnocky & Davis (1989) investigated the influence of pressure-dependent density and viscosity on the elastohydrodynamic collision of two spheres and showed that the pressure buildup during the collision process becomes sufficiently large so that the corresponding viscosity increase causes the interstitial fluid to behave nearly as a solid and to limit the close approach of the surfaces. Thus, the approaching sphere can be considered to have a virtual radius larger than the physical value. When the gap between the sphere and the target wall decreases to $\delta_{\rm ss}$, the virtual sphere with the effective radius $a' = a + \delta_{\rm ss}$ begins to reach the wall. Thus the elastic-like force starts to take effect at that moment so that the combined effect of elasticity and hydrodynamic forces resists the further approaching of the sphere. This effective radius becomes larger (increase from 0.0170 to 0.0178) for the collisions with smaller Stokes numbers (less than 30) in which the liquid is more viscous. In another word, the sphere starts to deform earlier and cannot penetrate as further as before. Similar concept was employed by Nguyen & Ladd (2002) who proposed a hydrodynamics radius for particles approaching another solid boundary to account for the lubrication layer effect; the hydrodynamics radius is $a_{hy} = a + \triangle$ and the value of $\triangle$ varies from 0 to $0.05a$ depending on the viscosity of the fluid and the particle radius a.

5.7 Coefficient of restitution

The coefficient of restitution, defined by the ratio of the rebound velocity V_r to the impact velocity V_i, $e = V_r/V_i$, is an important parameter that describes a collision in which the effects of the interstitial fluid are important. Here, the dependence of the coefficient of restitution on the Stokes number is computed from the simulation to evaluate the proposed contact model for immersed particle-wall collision process. To calculate the coefficient of restitution from the current simulations, consider the comparison between the simulated trajectory and the measured trajectory when the particle

is about to collide the wall shown in figure (5.8). Although the overall profile and the maximum height achieved in the rebound process from the simulation fit the experimental result as shown in figure (5.3), the simulated trajectory deviates from the measured trajectory during the short collision process to avoid the singularity problem arising when the two solid surfaces are too close. The deviation is the result of the proposed contact model.

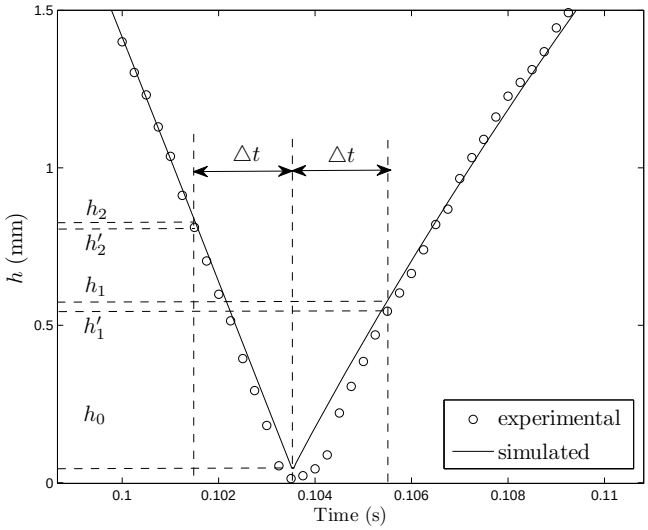

Figure 5.8: Particle trajectory when it is close to the wall

The coefficient of restitution for the simulated trajectory, denoted by e_s, is:

$$e_s = \frac{V_{rs}}{V_{is}} = \frac{(h_1 - h_0)/\triangle t}{(h_2 - h_0)/\triangle t} = \frac{h_1 - h_0}{h_2 - h_0} \tag{5.1}$$

where $\triangle t = 2$ ms; h_0, h_1, and h_2 are the gap values defined in figure (5.8) as the positions of the sphere at 2 ms after and before it reaches the lowest point h_0 in the simulation, respectively.

However, the actual coefficient of restitution for the measured trajectory is:

$$e = \frac{V_r}{V_i} = \frac{h'_1/\triangle t}{h'_2/\triangle t} = \frac{h'_1}{h'_2} \tag{5.2}$$

where h'_1 and h'_2 are the measured position of the sphere at 2 ms before and after it reaches the wall

in the experiment. The two results are different and they can be compared as:

$$\begin{aligned}\frac{e_s}{e} &= \frac{(h_1-h_0)/(h_2-h_0)}{h_1'/h_2'} = \frac{h_1-h_0}{h_1'}\frac{h_2'}{h_2-h_0} \\ &\simeq \frac{h_1h_2-h_2h_0}{h_1h_2-h_1h_0} = \frac{h_1h_2-h_1h_0+h_1h_0-h_2h_0}{h_1h_2-h_1h_0} \\ &= 1+\frac{(h_1-h_2)h_0}{(h_2-h_0)h_1}\end{aligned}$$

where an approximation is taken as $h_2' \simeq h_2$ and $h_1' \simeq h_1$ since the simulated trajectory only deviates from the experimental result when the sphere is very close to the wall. The relation between these gap values are: $h_1 \leq h_2$ since $e = h_1/h_2 \leq 1$; $h_2 > h_0$ otherwise the impact velocity is zero in the simulation. Then

$$\frac{e_s}{e} \leq 1$$

The coefficient of restitution for the simulated trajectory e_s is smaller than the experimental result e.

Thus, to compare with the current experiments and the other researcher's results, the coefficient of the restitution e is calculated as:

$$e = \frac{h_1}{h_2} \tag{5.3}$$

where h_2 and h_1 are the approximation of h_2' and h_1', respectively.

The impact Reynolds number and Stokes number is calculated based on a similar idea. The value of V_i is calculated from the simulation as:

$$V_i = \frac{h_2}{\triangle t}. \tag{5.4}$$

And correspondingly,

$$Re = \frac{DV_i}{\nu}, \tag{5.5}$$

$$St = \frac{m_pV_i}{6\pi\mu a^2} = \frac{1}{9}\frac{\rho_p}{\rho_l}Re. \tag{5.6}$$

The approximation of $h_2' \simeq h_2$ and $h_1' \simeq h_1$ might cause a slight difference between the calculated coefficient of restitution and the value measured from the experiments. To examine the difference, the results obtained by using equation (5.2) and (5.3) are compared in figure (5.9) for the first two impacts in the seven experimental cases described in Table (2.2).

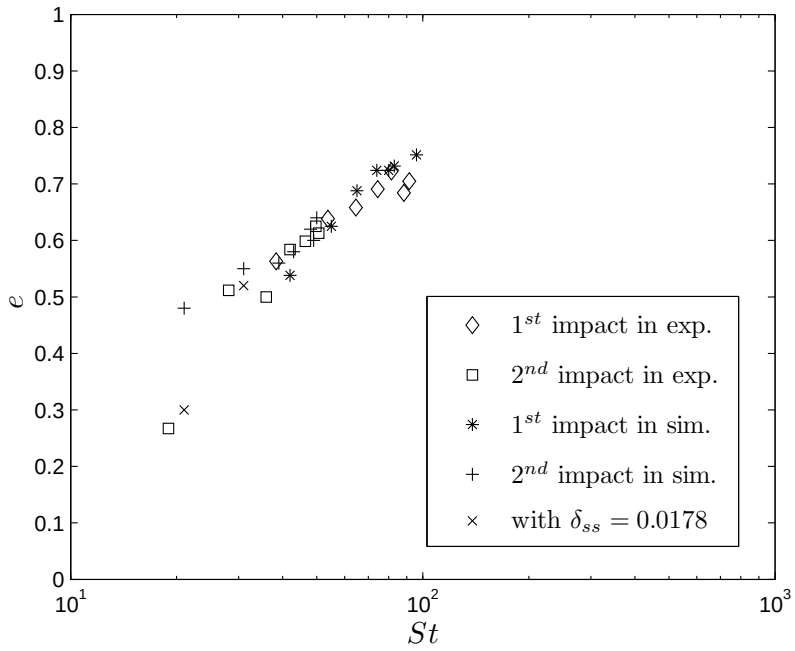

Figure 5.9: The coefficient of restitution for the first two impacts in the cases described in Table (2.2).

Figure (5.9) shows that the two sets of results are close for most of the cases with Stokes number greater than 30. The slight difference on Stokes number results from the approximation of $h_2' = h_2$ in calculating the impact velocity by using equation (5.4). The results for the second impacts of case 1 and 2 with Stokes number smaller than 30 are higher. As discussed in section (5.5), the simulated trajectory deviates from the experimental result when using $\delta_{\rm ss} = 0.017$ in the simulation for the collisions with Reynolds number less than 40 (corresponding Stokes number approximately less than 30). A larger value of $\delta_{\rm ss}$, $\delta_{\rm ss} = 0.017 + 5\%$ results in a trajectory with much lower relative error. When using the simulated trajectory with $\delta_{\rm ss} = 0.017 + 5\%$, the calculated coefficient of restitutions are closer to the experimental value as shown by the two cross points in figure (5.9). Thus, the coefficient of restitution calculated from equation (5.3) based on the simulation result can

run	ρ_l(g·cm^{-3})	μ(cP)	ρ_p(g·cm^{-3})	E(GPa)	ν	comment
1-3	1.17	15.2	7.6	200	0.33	steel sphere, 65% glycerol
4-10	1.20	50.0	7.6	200	0.33	steel sphere, 78% glycerol
11-14	1.20	50.0	11.35	16	0.44	lead sphere, 78% glycerol
15	1.20	50.0	24.0	200	0.33	artificial sphere, 78% glycerol
16	1.20	50.0	36.0	200	0.33	artificial sphere, 78% glycerol
17	1.20	50.0	48.0	200	0.33	artificial sphere, 78% glycerol
18-24	1.22	109	7.6	200	0.33	steel sphere, 85% glycerol
25-29	1.25	523	7.6	200	0.33	steel sphere, 95% glycerol
30-32	1.22	109	7.6	200	0.33	steel sphere, 85% glycerol

Table 5.1: Simulations with different input parameters and the corresponding material description. Runs with the same material properties have different initial distance; thus, the impact Stokes numbers are different. For the viscosity unit, 1 cP = 1×10^{-3} Pa·s.

be considered good approximation for the actual coefficient of restitution that represents the effect of the surrounding liquid on a collision process.

To examine the current contact model over a larger range of impact Stokes numbers and to compare with more experimental results found in the literature, simulations were run for denser particles and glycerol-water mixtures with different viscosity. The input parameters for each of the simulations are described in Table (5.1). For the runs with the same material properties, the initial distance between the sphere and the wall is set to be different so that the impact Reynolds number and Stokes number are different. In runs 15, 16 and 17, a sphere with an artificially large density is used to observe larger values of Stokes number (up to about 1000) while keeping the Reynolds number below 250 to ensure that the flow field remains axisymmetric. For runs 1 to 29, $\delta_{ss} = 0.017$ is used in the contact model. As a comparison, in runs 30, 31 and 32 that have the same initial condition and material properties as used in runs 18, 19 and 20, $\delta_{ss} = 0.017 + 5\%$ is used in the contact model, which results in different coefficient of restitution for impact Stokes number ranging from 10 to 30. The dimensionless distance δ_0, the corresponding Reynolds number Re, the Stokes number St and the coefficient of restitution e calculated from equation (5.3) based on the simulated result are listed in Table (5.2).

run	δ_0	Re_I	St_I	e	run	δ_0	Re_I	St_I	e
1	0.30	121	100	0.71	18	0.60	22	18	0.46
2	0.50	171	141	0.77	19	1.00	30	25	0.49
3	1.00	241	198	0.79	20	1.60	37	30	0.52
4	0.58	58	42	0.54	21	2.00	42	34	0.53
5	1.10	77	55	0.63	22	3.00	50	40	0.53
6	1.60	90	65	0.69	23	4.00	55	44	0.56
7	2.06	103	74	0.72	24	5.00	59	48	0.59
8	2.66	111	80	0.72	25	2.00	4.5	3.6	0.00
9	2.98	116	83	0.73	26	3.00	5.8	4.6	0.01
10	3.75	134	96	0.75	27	4.00	6.1	4.9	0.02
11	3.75	140	147	0.77	28	5.00	6.4	5.1	0.00
12	5.00	158	166	0.80	29	6.00	6.5	5.2	0.01
13	6.00	169	177	0.79	30	0.60	22	18	0.23
14	7.00	178	188	0.82	31	1.00	30	25	0.31
15	6.00	201	445	0.90	32	1.60	37	30	0.34
16	6.00	213	705	0.97	-	-	-	-	-
17	6.00	217	961	0.99	-	-	-	-	-

Table 5.2: Results of the different simulations.

The coefficient of restitution is plotted as a function of Stokes number as shown in figure (5.10). For runs 15, 16 and 17 with large Stokes number ($400 \sim 10^3$), the coefficient of restitution approaches to the dry value e_d, which indicates the liquid effect is becoming negligible and the elastic force plays the main role and makes the sphere rebound as in a dry collision process. When the Stokes number is in the range of $10 \sim 200$, the hydrodynamic forces exert more effect on the particle and the coefficient of restitution decreases as the Stokes number decreases. For runs 25-29, a higher liquid viscosity was used so that the kinetic energy of the sphere is dissipated by viscous effects from the liquid-solid interaction term. The impact velocity is small and the corresponding impact Stokes number is smaller than 10. There is no rebound and the coefficient of restitution is zero. Thus, the combined effect of the hydrodynamic force term and the elastic-like force term lead to a complete contact model for a impact Stokes number from 1 to 1000.

The relation between the coefficient of restitution calculated from the current simulations and

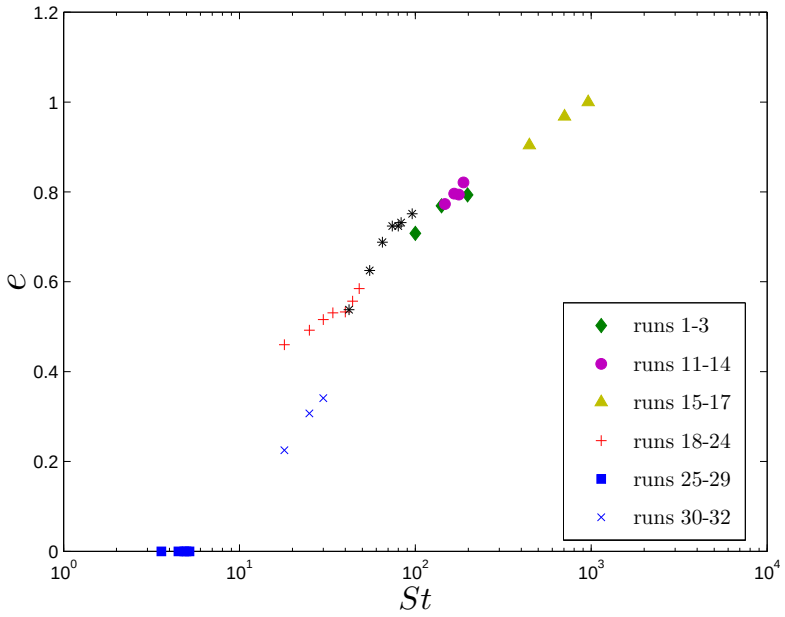

Figure 5.10: Simulation results of coefficient of restitution as a function of Stokes number.

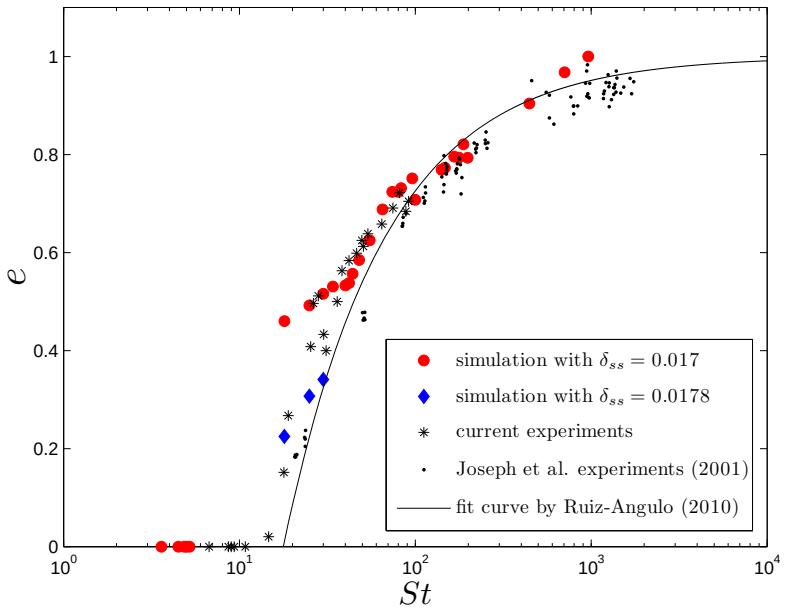

Figure 5.11: Comparison of the relations between coefficient of restitution and particle Stokes number.

the particle impact Stokes number agrees with the empirical trend, as shown in figure (5.11) that compares the simulated results with the measured results from the current experiments and Joseph et al.'s pendulum experiments [2001] for a steel sphere and Zerodur wall. For Stokes number ranging from 90 to 200, the values of the coefficient of restitution calculated from the current simulations overlap with the experimental results of Joseph *et al.* (2001) even though the whole flow field configurations are different (the sphere falls under gravity and collides with the wall vertically in the simulations while in Joseph et al.'s pendulum experiments the sphere collides with the wall horizontally). For Stokes number ranging from 30 to 90 where Joseph *et al.* (2001) has fewer experimental points, the simulated results overlap with the measured results from the current experiments. For Stokes number ranging from 10 to 30, the coefficient of restitution increases with large slope with increasing St and the experimental data are scattered within the small range of Stokes number. The results obtained from the simulations are sensitive to the non-dimensional parameter δ_{ss}. When using $\delta_{\text{ss}} = 0.017 + 5\%$ the simulations produce the coefficient of restitutions that follow the trend of a fit curve of the experiment data in Joseph *et al.* (2001) and Gondret *et al.* (2002) given by Ruiz-Angulo & Hunt (2010) as $e_{fit} = 1 - 8.65/St^{0.75}$.

In summary, the different material properties including the solid elastic property, liquid viscosity and the density ratio are incorporated appropriately in the proposed contact model. The current simulations represent the dependence of the coefficient of restitution on the impact particle Stokes number demonstrating that the contact model captures the essential physics of a particle-wall collision process in a liquid environment.